

DTIC

AGE

Form Approved
OMB No 0704 01RB

1a REPORT SECURITY CLASSIFICATION Unclassified		AD-A237 508		RESTRICTIVE MARKINGS	
2a SECURITY CLASSIFICATION				DISTRIBUTION/AVAILABILITY OF REPORT	
2b DECLASSIFICATION/CONTROLLING AGENCY				Approved for public release and sale; its distribution is unlimited.	
4 PERFORMING ORGANIZATION REPORT NUMBER(S) Technical Report No. 106			5. MONITORING ORGANIZATION REPORT NUMBER(S)		
6a NAME OF PERFORMING ORGANIZATION Purdue University Department of Chemistry		6b. OFFICE SYMBOL (if applicable)	7a. NAME OF MONITORING ORGANIZATION Division of Sponsored Programs Purdue Research Foundation		
6c ADDRESS (City, State, and ZIP Code) Purdue University Department of Chemistry West Lafayette, IN 47907		7b. ADDRESS (City, State, and ZIP Code) Purdue University West Lafayette, IN 47907			
8a NAME OF FUNDING / SPONSORING ORGANIZATION Office of Naval Research		8b OFFICE SYMBOL (if applicable)	9 PROCUREMENT INSTRUMENT IDENTIFICATION NUMBER Contract No. N00014-91-J-1409		
8c ADDRESS (City, State, and ZIP Code) 800 N. Quincy Street Arlington, VA 22217		10. SOURCE OF FUNDING NUMBERS			
		PROGRAM ELEMENT NO.	PROJECT NO.	TASK NO.	WORK UNIT ACCESSION NO.
11 TITLE (Include Security Classification) Atomic-Resolution Scanning Tunneling Microscopy and Infrared Spectroscopy as Combined In-Situ Probes of Electrochemical Adlayer Structure: Carbon Monoxide on Rhodium(111)					
12 PERSONAL AUTHOR(S) S.-L. Yau, X. Gao, S.-C. Chang, B.C. Schardt, and M.J. Weaver					
13a TYPE OF REPORT Technical		13b TIME COVERED FROM _____ TO _____		14. DATE OF REPORT (Year, Month, Day) May 31, 1991	15. PAGE COUNT
16 SUPPLEMENTARY NOTATION					
17. COSATI CODES			18. SUBJECT TERMS (Continue on reverse if necessary and identify by block number)		
FIELD	GROUP	SUB-GROUP	In-situ scanning tunneling microscopy and infrared reflection-adsorption spectroscopy, atomic-level adlayer structures, carbon monoxide on Rh(111)		
19 ABSTRACT (Continue on reverse if necessary and identify by block number) In-situ scanning tunneling microscopy (STM) has been combined with infrared reflection-adsorption spectroscopy (IRRAS) to yield detailed atomic-level adlayer structures for saturated coverages of CO on ordered Rh(111) in aqueous solutions. Two distinctly different structures were obtained in CO-containing 0.1 M NaClO₄, depending on the electrode potential. At higher potentials, ca -0.1 to 0.3 V vs SCE, atomic-resolution STM images were obtained that indicated the presence of a (2 x 2)-3CO unit cell, having a CO coverage $\theta_{CO} = 0.75$ in agreement with electrochemical and IRRAS measurements. The corresponding in-situ infrared spectra indicate the presence of two atop (or near-atop) and one twofold bridging CO in the unit cell. A real-space structure is suggested that is related to the corresponding (2 x 2)-3CO adlattice on Rh(111) in uhv as deduced previously by low-energy electron diffraction and vibrational spectroscopy. At potentials negative of -0.2 to -0.1 V vs SCE, markedly different STM images were obtained, having the symmetry (3 x $\sqrt{3}$ rect)-4CO ($\theta_{CO} = 0.67$). This reversible potential-induced structural alteration as discerned by STM correlates with the					
20 DISTRIBUTION/AVAILABILITY OF ABSTRACT <input type="checkbox"/> UNCLASSIFIED/UNLIMITED <input type="checkbox"/> SAME AS RPT. <input type="checkbox"/> DTIC USERS			21. ABSTRACT SECURITY CLASSIFICATION		
22a NAME OF RESPONSIBLE INDIVIDUAL			22b TELEPHONE (Include Area Code)	22c OFFICE SYMBOL	

Accession For	
GRAB	<input checked="" type="checkbox"/>
BTIC Tab	<input type="checkbox"/>
Unassigned	<input type="checkbox"/>
Justification	
By	
Distribution/	
Availability Codes	
Dist	Avail and/or Special
A-1	



19. (cont.)

substantial changes observed in the infrared spectra. The latter indicate the predominant presence of bridging CO in the (3 x √3 rect) structure, with only one CO per unit cell being coordinated at an atop site. Both the STM images and the IRRAS data suggest that two CO's occupy "asymmetric bridging" positions. The increased preference for bridge bonding at lower potentials is consistent with the greater extent of $d\pi - 2\pi^*$ metal-CO back bonding expected under these conditions. The virtues of parallel STM and IRRAS measurements for deducing ordered adlayer structures of such unprecedented atomic-level detail at metal-solution interfaces are emphasized.

91-03196



91 03 196

OFFICE OF NAVAL RESEARCH

Contract No. N00014-91-J-1409

Technical Report No. 106

Atomic-Resolution Scanning Tunneling Microscopy
and Infrared Spectroscopy as Combined In-Situ Probes of
Electrochemical Adlayer Structure: Carbon Monoxide on Rhodium(111)

by

S.-L. Yau, X. Gao, S.-C. Chang, B.C. Schardt, and M.J. Weaver

Prepared for Publication

in the

Journal of American Chemical Society

Purdue University

Department of Chemistry

West Lafayette, Indiana 47907

May 1991

Reproduction in whole, or in part, is permitted for any purpose of the United States Government.

* This document has been approved for public release and sale: its distribution is unlimited

**Atomic-Resolution Scanning Tunneling Microscopy and Infrared
Spectroscopy as Combined In-Situ Probes of Electrochemical Adlayer**

Structure: Carbon Monoxide on Rhodium (111)

Shueh-Lin Yau, Xiaoping Gao, Si-Chung Chang,

Bruce C. Schardt[‡] and Michael J. Weaver*

Department of Chemistry, Purdue University

West Lafayette, Indiana 47907

[‡] Current address: Department of Physics, Brookhaven National Laboratory,
Upton, NY 11973

J. Am. Chem. Soc.

submitted February 12, 1991

revised April 5, 1991

ABSTRACT

In-situ scanning tunneling microscopy (STM) has been combined with infrared reflection-absorption spectroscopy (IRRAS) to yield detailed atomic-level adlayer structures for saturated coverages of CO on ordered Rh(111) in aqueous solutions. Two distinctly different structures were obtained in CO-containing 0.1 M NaClO₄, depending on the electrode potential. At higher potentials, ca -0.1 to 0.3 V vs SCE, atomic-resolution STM images were obtained that indicated the presence of a (2 x 2)-3CO unit cell, having a CO coverage $\theta_{CO} = 0.75$ in agreement with electrochemical and IRRAS measurements. The corresponding in-situ infrared spectra indicate the presence of two atop (or near-atop) and one twofold bridging CO in the unit cell. A real-space structure is suggested that is related to the corresponding (2 x 2)-3CO adlattice on Rh(111) in uhv as deduced previously by low-energy electron diffraction and vibrational spectroscopy. At potentials negative of -0.2 to -0.1 V vs SCE, markedly different STM images were obtained, having the symmetry (3 x $\sqrt{3}$ rect)-4CO ($\theta_{CO} = 0.67$). This reversible potential-induced structural alteration as discerned by STM correlates with the substantial changes observed in the infrared spectra. The latter indicate the predominant presence of bridging CO in the (3 x $\sqrt{3}$ rect) structure, with only one CO per unit cell being coordinated at an atop site. Both the STM images and the IRRAS data suggest that two CO's occupy "asymmetric bridging" positions. The increased preference for bridge bonding at lower potentials is consistent with the greater extent of $d\pi - 2\pi^*$ metal-CO back bonding expected under these conditions. The virtues of parallel STM and IRRAS measurements for deducing ordered adlayer structures of such unprecedented atomic-level detail at metal-solution interfaces are emphasized.

A major goal in surface electrochemistry is the attainment of molecular- (or atomic-) level information on adsorbate structure at metal-solution interfaces. As for surface science in ultrahigh vacuum (uhv), it is desirable to utilize oriented monocrystalline metals for this purpose, so to yield ordered and stereochemically uniform interfaces. Tactics involving electrode emersion and transferral to uhv have been used extensively for adsorbate characterization, exploiting the range of surface structural techniques available in the latter environment.¹ Nevertheless, such "ex-situ" approaches are limited inherently by the drastic changes in system state that can occur upon surface transfer, with attendant alterations in interfacial structure.

As a consequence, the development of in-situ characterization methods in electrochemical surface science is garnering considerable attention. Of the various candidates, both scanning tunneling microscopy (STM) and surface vibrational spectroscopies, especially infrared reflection-absorption spectroscopy (IRRAS), have much to offer for the elucidation of adsorbate structure, yet in manifestly different ways. At least in suitable cases, STM has recently proven capable of providing atomic-resolution images of ordered adlayers on monocrystalline metals in aqueous electrochemical environments.^{2,3} While IRRAS provides little information on such real-space structural arrangements, detailed insight into adsorbate surface bonding and orientation can be obtained from vibrational frequencies, relative intensities and bandshapes. Although most electrochemical applications of IRRAS have involved polycrystalline surfaces, studies on ordered monocrystalline metals are becoming prominent.⁴ Given the complementary structural information provided by these techniques, interesting opportunities are emerging for their application in tandem to explore electrochemical adlayer structure at a level previously exclusive to uhv surface science.

An adsorbate of unique significance in surface science is carbon monoxide; this species has additional relevance to electrochemical systems as a common poison in the catalytic electrooxidation of organic fuels.⁵ Recently, the possibility of obtaining in-situ atomic-resolution STM images of close-packed CO adlayers in electrochemical systems has been demonstrated by two of us, initially for CO on Pt(111) in aqueous 0.1 M HClO₄.³ Infrared spectroscopy is also well suited to the structural characterization of adsorbed CO in view of the well-known sensitivity of the C-O stretching frequency, ν_{CO} , to the surface coordination geometry. Indeed, along with low-energy electron diffraction (LEED) such vibrational data have formed a cornerstone in studies of CO adlayer structures in metal-uhv systems.^{6,7} Similarly to LEED, the STM technique can provide detailed information on the symmetry and unit-cell dimensions of the adlayer, but cannot identify the surface binding sites. The infrared spectra therefore can provide this additional information necessary to deduce the CO adlayer structure.

These considerations trigger the prospect of employing parallel in-situ STM and IRRAS data to generate benchmark adlayer structures along the lines already established for metal-uhv systems with LEED and IRRAS.^{6,7} The potential-, as well as coverage-, dependent adsorption of CO on low-index platinum and rhodium electrodes in aqueous media has recently been examined in detail using IRRAS in our laboratory.^{4,8-12} The CO binding geometries can depend significantly on the electrode potential, in several cases signaling adlayer structures that are quite different to those observed in the corresponding anhydrous uhv environment.^{4,11} These interesting disparities can be understood primarily in terms of the differences in surface potential between the electrochemical and uhv systems.⁴

A surface of particular interest in this regard is Rh(111). At relatively positive potentials, the ν_{CO} spectra at saturation CO coverage ($\theta_{CO} = 0.75$) are closely reminiscent of vibrational measurements in uhv, which exhibit a major ν_{CO}

band due to atop coordination and a weaker feature consistent with the presence of a twofold bridging site.^{10a,11} At lower potentials, negative of ca 0 V vs saturated calomel electrode (SCE), a dramatic yet reversible structural change occurs, with the CO shifting to a predominantly bridging coordination.¹¹ Such potential-induced structural transformations can generally be understood from the greater degree of metal-CO $d\pi - 2\pi^*$ back donation, associated with such multiple CO coordination, favored at more negative potentials and correspondingly larger surface charges.^{4a,13}

This raises the intriguing question of how such potential-induced changes in CO binding geometry are reflected in corresponding alterations in the real-space adlayer structures as can be discerned from STM. Reported herein are atomic-resolution STM images for saturated ($\theta_{CO} \approx 0.75$) CO adlayers on Rh(111) in aqueous 0.1 M NaClO₄ and 0.1 M HClO₄. The potential-dependent STM data are combined with IRRAS measurements obtained under the same conditions to yield adlayer structural information of unprecedented atomic-level detail for electrochemical surfaces. Comparisons are made with adlayer structures deduced for the corresponding Rh(111)/CO and related systems in uhv.^{14,15}

EXPERIMENTAL SECTION

The Rh(111) crystal used for both the STM and IRRAS measurements (9mm diameter, 4mm thick) was obtained from the Materials Preparation Facility of Cornell University; it was oriented within $\pm 1^\circ$. Electrical contact was via Pt wires spot welded to the back of the crystal. Preparation of a well-ordered surface for in-situ electrochemical purposes was achieved by means of the procedure outlined in ref. 10 (cf ref. 16). Briefly, this entails annealing to glowing red in a hydrogen-air flame, followed by rapid transfer to a nitrogen atmosphere above iodine crystals. The iodine protective layer thus formed was then replaced by CO subsequently in a flushable electrochemical cell. The

adsorbed CO can then be removed by voltammetric electrooxidation in 0.1 M HClO₄, exposing the "butterfly" voltammetric features characteristic of a clean well-ordered Rh(111) surface. Figure 1 (dashed trace) shows a typical voltammogram at 50 mV s⁻¹ for ordered Rh(111) in 0.1 M NaClO₄; the solid trace is a preceding voltammogram for the electrooxidation of irreversibly adsorbed CO. After satisfactory voltammograms were obtained, the surfaces were transferred rapidly to the STM or IRRAS cell, as appropriate (vide infra).

Some experimental details of the STM measurements have been presented previously.^{2,17-19} The microscope is a commercial Nanoscope II instrument with a bipotentiostat (Digital Inc.) so to perform in-situ electrochemical STM. (The bipotentiostat allows the potential of the substrate surface and the STM tip to be varied both with respect to each other and to the reference electrode). The STM tip is held at virtual ground. For electrochemical experiments involving variations in the substrate (working electrode) potential, E_{we} , it is usually convenient to hold the tip-surface bias voltage V_b fixed, so that parallel variations occur in the tip electrode potential, E_{tip} (but see below). Values of V_b were typically from +200 to -200 mV, with set-point currents, i_t , of ca 10-20 nA, although conditions were varied in each experiment with the primary objective to optimize image quality. (See appropriate figure captions for specific details). The atomic-resolution images were generally obtained by using the "constant height" mode. Where appropriate, the atomic-scale images were filtered by using the 2d-FT program in the Nanoscope software.

The STM electrochemical cell was machined from a cylindrical ring of Kel-F. The open bottom of the cell (internal diameter 7.5mm) was sealed to the Rh(111) surface by a steel compression fitting screwed into the base of the microscope. Due to the size constraints of the STM cell, an oxidized gold wire was employed as a quasi-reference electrode. It was prepared by oxidizing anodically the wire

in a separate 0.1 M HClO₄ solution (at ca 3.0 V vs Pt wire) prior to use. The potential of this "Au/AuO" electrode in 0.1 M NaClO₄ is about 0.8 V positive of the saturated calomel electrode (SCE); however, its stability (generally within 0.1 V in a given solution) was checked periodically during experiments by measuring the onset potential of cathodic hydrogen evolution. The tungsten tunneling tips were 0.010in wires etched to a sharp point in 1 M KOH. After mounting in the tunneling head, the wire was insulated electrically by painting with clear nail polish ("Wet 'n Wild", Pavion Ltd.).²

Details of the electrochemical IRRAS measurements are largely as described in refs. 9a and 20. The FTIR spectrometer is an IBM (Bruker) IR-98-4A instrument, with a Globar light source and a MCT narrow-band detector (Infrared Associates). The thin-layer spectroelectrochemical cell utilized a CaF₂ window bevelled at 60° to the surface normal so to optimize the effective angle of incidence of the light beam onto the electrode surface.^{9a}

Carbon monoxide (99.8%) was obtained from Matheson, perchloric acid (double distilled) and sodium perchlorate (recrystallized) from G.F. Smith, and potassium hydroxide (Ultrapure grade) from Alfa. Water was purified by means of a Milli-Q system (Millipore Inc.). All electrode potentials are quoted here versus the SCE.

RESULTS

IRRAS Measurements

Our electrochemical IRRAS studies of CO on Rh(111),^{10a,11} as for other surfaces, have been concerned chiefly with irreversibly adsorbed adlayers (i.e., following removal of solution CO), primarily to ease interpretation of the corresponding voltammetric data. In the present in-situ STM experiments, however, it is more practical to examine CO adlayers in the presence of near-saturated (ca 1 mM) CO solutions. Consequently, additional IRRAS data that refer

to the latter condition have been gathered in the present work.

Figure 2 shows a typical sequence of potential-dependent infrared spectra obtained within the ν_{CO} frequency region for Rh(111) in CO-saturated 0.1 M NaClO₄. The initial potential, -0.4 V vs SCE, is close to the onset of hydrogen evolution in this electrolyte. The upward-going spectral sequence was obtained, as before, by acquiring sets of interferometer scans as the potential is swept slowly positive (at 1 mV s⁻¹). Each spectrum in Fig. 2, referring to the average potentials indicated, was acquired from 100 interferometer scans, the solvent interference being removed by subtracting a similar set obtained following complete CO electrooxidation, at ca 0.5 V.

A notable feature of Fig. 2 is the marked potential-induced changes in CO site occupancy. At the most negative potentials, a major band at 1885-1900 cm⁻¹ is seen along with a weaker feature at 2010-2020 cm⁻¹, consistent with CO bound in "asymmetric twofold" (vide infra) and atop configurations, respectively.^{10a,11} Between ca -0.2 and -0.1 V, however, the adlayer structure alters markedly to one featuring predominantly atop (or near-atop) coordination, as evidenced by the major feature at 2030-2045 cm⁻¹, along with a weaker band at 1800-1820 cm⁻¹ indicating the additional presence of twofold bridging CO. [Note that the progressive ν_{CO} frequency upshifts seen for increasing potentials in Fig. 2 occur even at fixed site occupancy, being associated with electrostatic field (first-order Stark) and/or metal-adsorbate charge-transfer effects.^{4a,21}] These changes in CO site occupancy were found to occur in near-reversible manner by altering the potential across the range ca -0.2 to -0.05 V vs SCE. The data in Fig. 2 are similar to those in Fig. 3 of ref. 11, yet show subtle differences arising from the presence of solution CO. In particular, the loss of the asymmetric bridging CO towards more positive potentials is more clearcut under the present conditions (Fig. 2).

Infrared spectra were also obtained for CO-saturated solutions in acidic perchlorate media, such as 0.1 M HClO₄ or 0.1 M NaClO₄ + 5 mM HClO₄. Qualitatively comparable potential-induced adlayer structural changes were observed in these solutions as in neutral (0.1 M NaClO₄) media; however, the formation of the "lower-potential" spectral features was incomplete even at the most negative potentials (ca -0.3 V) that can be accessed in such acidic media.

STM Measurements

The protocol for transferring the Rh(111) crystal from the electrochemical cell to the STM cell was slightly different to that for the IRRAS measurements, necessitated by the need to mount the sample and bolt down the cell wall before introducing the electrolyte. The consequent short exposure of the surface to the atmosphere introduces the likelihood of significant surface contamination. This possibility was checked by exposing the freshly pretreated surface to air for 1-2 mins, followed by reimmersion in 0.1 M HClO₄ and further voltammetric and/or infrared characterization. Typically, the voltammetric features characteristic of a clean surface (Fig. 1, dashed trace) could be recovered essentially entirely by further potential cycling under these conditions. Reimmersion of the surface into CO-saturated solution tends to yield somewhat (ca 20%) lower CO coverages than for fresh surfaces, as indicated most directly from the infrared intensities, even though the local adlayer structure apparently remained unaffected as discerned from the identical form of the spectral features. We therefore have some confidence that the STM and IRRAS data indeed refer to comparable states of the Rh(111) surface.

The usual procedure for in-situ STM involved filling immediately the Kel-F cup with CO-saturated electrolyte with the Rh(111) electrode potential held at about -0.1V vs SCE. Voltammetric sweeps were conducted in this environment periodically to check the stability of the Au/AuO quasi-reference electrode and

the retention of sufficient CO in the electrolyte. (Note that oxygen could not be excluded entirely from the STM cell during experiments, although the entire arrangement was surrounded by a metal cover which could be blanketed with helium.) In view of the above IRRAS data, the majority of STM experiments were performed in 0.1 M NaClO₄, although some data were also obtained in 0.1 M HClO₄.

Examination of the STM topographical features revealed large-scale terraces, averaging 500Å in width. Within these terraces, three distinct atomic-resolution patterns could be obtained. The first was observed occasionally on portions on these terraces, especially at relatively positive potentials (ca 0.5-0.6 V) in 0.5 M NaClO₄, where CO electrooxidative removal has occurred. A typical topview image is shown in Fig. 3. The distance between adjacent spots (2.7-2.8Å) together with the hexagonal close-packed structure identify the image as arising from the substrate surface atoms, i.e., Rh(111)-(1 x 1). The direction of the hexagonal substrate structure (in the xy plane) as discerned from the image in Fig. 3 is also in good agreement with independent information obtained by x-ray back-diffraction. (The crystal was mounted consistently in the STM cell so that the substrate lattice direction as deduced from x-ray diffraction is known, thereby enabling it to be compared with the adlayer images noted below.)

Two distinctly different types of STM images were obtained in potential regions where CO is stable towards electrooxidation. At electrode potentials positive of ca -0.2 V in CO-saturated 0.1 M NaClO₄ (or 0.1 M HClO₄), images having (2 x 2) symmetry with respect to the substrate lattice were obtained. Typical topview images of this type are depicted in Figs. 4A-C. Figure 4A shows a relatively extended (80 x 80Å) domain, as an example of an unfiltered STM image of this type. An expanded (25 x 25Å) and mildly filtered portion of the same image is given in Fig. 4B; a 3d "height-shaded surface plot" of the same image,

with a viewpoint 30° off the surface normal, is pictured in Fig. 4C. Within the (2×2) unit cell (as drawn in Fig. 4B), three distinct yet nonequivalent spots can be discerned. This information suggests that the image arises from a CO adlattice of structure (2×2) -3CO, having a coverage, θ_{CO} , of 0.75. Interestingly, this coverage is equal to the value obtained from infrared and electrochemical data;^{10a,11} the same saturation coverage is obtained for the Rh(111)/CO uhv system, which also features a (2×2) unit cell (vide infra).¹⁴ Also, a "split" (2×2) LEED pattern, presumably reflecting the presence of (2×2) domains, is observed for lower CO coverages on Rh(111) surfaces emersed from aqueous 0.1 M HClO_4 at ca 0.1 V vs SCE .¹⁵

The asymmetric nature of the (2×2) STM image in Fig. 4A-C suggests that other domains should be observable having the same symmetry but rotated and/or inverted with respect to the former image. Such rotated domains were indeed observed, even though their detection was hampered somewhat by a commonly inability to resolve entirely all three STM spots in the unit cell. One example of an unusually well-resolved, yet reproducible, domain image is shown in Fig. 4D. This image can be virtually superimposed on that in Fig. 4B by 60° counterclockwise rotation and inversion.

At potentials negative of ca -0.2 V in CO-saturated 0.1 M NaClO_4 , domains having a markedly different atomic-resolution STM image were favored, as illustrated in Figs. 5A-D. Figure 5A consists of a typical $25 \times 25 \text{ \AA}$ topview image of this structure, and Fig. 5B is a corresponding "height-shaded surface plot" obtained from the same data. By comparison with the substrate lattice dimensions and direction (Fig. 3), this structure can be identified as $(3 \times \sqrt{3} \text{ rect})$ -4CO; a unit cell is drawn in Fig. 5A. Four distinct spots can be discerned, the "brightest" being at the edge of the unit cell as drawn. If again each spot is associated with one CO, a coverage of $2/3$ (i.e., $\theta_{\text{CO}} = 0.67$) is

deduced.

The ($3 \times \sqrt{3}$ rect) images tend to display an interesting asymmetry in that a significant periodicity occurs, yielding "furrows" along the $\sqrt{3}$ direction towards the right-hand-side of the unit cell as drawn in Fig. 5A. The asymmetry may arise at least in part from an artifact associated with the direction of the tip scan. Given the hexagonal symmetry of the substrate surface atoms, one might anticipate the appearance of three distinct, yet equivalent, ($3 \times \sqrt{3}$) domain structures that are rotated 120° with respect to each other. Indeed, all three such domain types were observed; an example of an edge between a pair of such rotated domains is given in Fig. 5C. Significantly, the "furrows" noted above are more pronounced for domains where the tip scan direction (right to left along the x-axis on all images shown) is roughly normal to the observed corrugations. Conversely, the extent of these corrugations is markedly smaller for domains rotated 60° counterclockwise to that in Fig. 5A, where the tip scan direction more closely parallels this feature. An example of this latter circumstance is shown in Fig. 5D.

Ideally, it would be desirable of course to obtain STM images that contained information on *both* the adlayer and substrate atomic positions, enabling adsorbate binding sites to be discerned from STM. Such combined images have apparently never been reported, although substrate images have occasionally been obtained for surfaces in the presence of compressed adlayers.² For the present system, systematic variations in V_b and/or i_t at electrode potentials where the CO adsorbate is present yielded persistently adlayer, rather than substrate, images. The use of larger V_b and/or smaller i_t (so to increase the tip-surface separation) resulted in comparable images, although the components of the unit cell were less easily resolved. (Detailed discussion of the relationships between V_b , i_b , and the surface-tip separation for a related, yet

more reproducible metal-adsorbate system, Pt(111)-I, is to be found in ref. 19.)

A key feature of the present results is the correlation between the potential-induced changes in adlayer structures as discerned by STM and the corresponding IRRAS data. Experiments involving slow potential alterations while STM images were being recorded, as employed for IRRAS (Fig. 2), enabled a close correspondence between the potential-dependent STM and IRRAS phenomena to be established with confidence. Within the potential range ca -0.1 V to -0.2 V, both the (2×2) and $(3 \times \sqrt{3})$ structures could sometimes be observed in adjacent domains, the proportion of the former increasing towards higher (i.e., less negative) electrode potentials. An example of such a domain boundary is shown in Fig. 6, the upper and lower portions of the image consisting of $(3 \times \sqrt{3})$ and (2×2) domains, respectively. (The "blotches" seen clearly in this image were commonly obtained in some terrace regions, and probably arise from surface impurities and imperfections.) The best resolved images of the $(3 \times \sqrt{3})$ structure were often obtained by using larger positive bias voltages than utilized for observing the (2×2) structure. This arises from the lower E_w values at which the former structure is typically obtained, since it is desirable to hold E_{tip} at more positive values (i.e., yielding larger V_b) so to minimize stray faradaic currents at the STM tip. Nevertheless, as exemplified by Fig. 6, both the (2×2) and $(3 \times \sqrt{3})$ structures could be imaged with a given V_b value.

DISCUSSION

Given that this close correlation between the potential-dependent STM and IRRAS behavior provides strong support to the contention that the former data also arises from the CO adsorbate, the two data sets can be combined so to yield detailed insight into the real-space adlayer structures. The chief objective here is to identify specific binding sites on the Rh(111) surface for each CO in the unit cell.

We consider first the (2×2) -3CO structure, present on Rh(111) at more positive potentials. The proportion, as well as the nature of, each CO binding site can be extracted fairly directly from the infrared spectra in the following manner. As mentioned above, the higher- and lower-frequency ν_{CO} bands, occurring at 2030–2040 cm^{-1} and 1800–1820 cm^{-1} within the potential range ca -0.1 to 0.3 V where the (2×2) structure is stable (Fig. 2), can be identified with atop (or near-atop) and twofold bridging coordination, respectively. These binding-site designations are aided by the observation that extrapolation of the ν_{CO} frequency-electrode potential data to surface potentials equivalent to that for the Rh(111)/CO ($\theta_{\text{CO}} = 0.75$) uhv interface yields ν_{CO} frequencies, ca 2075 and 1870 cm^{-1} , closely similar to those observed (2070 and 1860 cm^{-1} ²²) for the latter system.^{4b,23} (As discussed recently in detail,^{4a} such extrapolations correct for the differing influences of electrostatic fields and metal surface charges within the electrochemical and uhv environments on the adsorbate vibrational frequencies.) The firm identification of the 2070 and 1860 cm^{-1} bands for the Rh(111)/CO ($\theta_{\text{CO}} = 0.75$) uhv system as arising from near-atop and symmetrical twofold bridging CO, respectively, has been made from a detailed dynamical LEED analyses combined with surface vibrational data as obtained by electron energy loss spectroscopy (EELS).¹⁴

The relative site occupancies of the atop (i.e., terminal) and bridging sites, (S_t/S_b), can be extracted approximately from the ratio of integrated absorbances, (A_t/A_b), combined with the corresponding ratio of infrared band absorptivities, (ϵ_t/ϵ_b). The last quantity has been determined to be ca 2 to 2.5 for related electrochemical and uhv systems.^{12a,24} Given that from Fig. 2, (A_t/A_b) = 4.7 (at 0.25 V), the site occupancy ratio (S_t/S_b) [$-(A_t/A_b)/(\epsilon_t/\epsilon_b)$] is determined to be ca 2. Consequently, then, two of the three CO's in the unit cell can be assigned to atop (or near-atop) sites, with the third in a twofold

bridging site. Interestingly, the same site occupancy applies to the Rh(111)/CO($\theta_{\text{CO}} = 0.75$) uhv system, as deduced both from the EELS and dynamical LEED data.¹⁴ Furthermore, the latter indicates the presence of a (2 x 2) unit cell, similar to that inferred for the corresponding electrochemical interface from the STM images (Fig. 4).

With this information in hand, likely real-space adlattice structures for the present (2 x 2)-3CO adlayer can be proposed. Such a topview "ball-model" structure, derived from the STM image in Fig. 4B, is shown in Fig. 7A. The top-layer Rh atoms are depicted as the larger circles, with the smaller circles representing individual CO molecules. (The CO's are bound via the carbon atom, with the C=O bond axis expected to be roughly parallel to the surface normal.) The corners of the unit cell included in Fig. 7A are intended to match that drawn on the STM image in Fig. 4B. The CO in the corner position in Fig. 7A is placed in a twofold bridging site so to correspond to the least intense of the trio of STM spots in Fig. 4B. This designation, although not entirely firm, is consistent with the expectation that tip-surface electron tunneling via adsorbate in bridging sites should be less efficient than via atop species (with the STM tip travelling at "constant height" above the substrate) simply because the former adsorbate is imbedded somewhat into the surface plane. [Such a prediction is in accordance with STM data for structurally well-defined iodine adlattices on Pt(111).^{17,19}]

On the basis of the infrared data, the two brighter STM spots within the unit cell in Fig. 4B can be assigned to CO's at atop, or near-atop, sites, and are depicted as such in Fig. 7A. There is, however, an interesting ambiguity as to the precise location of this CO pair. Simple stereochemical considerations would place these molecules in near-atop, rather than symmetrical atop, sites, so to minimize the adsorbate-adsorbate repulsions. Indeed, such a structure,

featuring the CO pair at near-atop sites both shifted ca 0.5\AA from the symmetrical atop position, is indicated from a dynamical LEED analysis for the $(2 \times 2)\text{-3CO}$ uhv system.¹⁴ However, such a geometric equivalence of the near-atop CO pair is apparently not entirely consistent with the form of the STM image, which displays a pair of spots of unequal brightness sited in nonequivalent positions within the unit cell (Fig. 4B). Geometric as well as spot-intensity considerations would place the left-hand CO closer to the edge of the unit cell as drawn in Fig. 7A. This choice, however, yields unusually (and probably unacceptably) small and non-uniform CO-CO distances within the unit cell. In particular, the shortest CO-CO distance in Fig. 7A is slightly smaller than the rhodium atomic diameter, 2.68\AA .

A possible resolution of this quandary lies in the realization that the CO pair, even when placed in *geometrically* equivalent near-atop sites (with respect to the substrate top layer), are liable to be electronically distinct in an STM experiment, since the rhodium second-layer atoms are displaced differently with respect to the adlayer molecules. (This point is readily evident upon inspecting Fig. 1 of refs. 14a or b.) Evidence for an important role of second-layer metal structure in STM has been gleaned previously for iodine adlayers on Pt(111).^{17,19} Such electronic effects may influence the STM image so that the STM spot positions, as well as intensities, may not always be an entirely reliable guide to precise adsorbate location, especially for molecular species. In general, STM is expected to probe the spatial variations in the Fermi-level density of states at the surface,²⁴ the maxima of which may not always be related precisely to adsorbate position. For example, adsorbed oxygen atoms have been calculated to yield negative corrugations in STM images under some circumstances.²⁵

Consequently, then, it is plausible that the actual position of at least the asymmetric atop CO's in the (2×2) structure differs significantly from that

inferred from the STM images (Fig. 7A). An alternative ball-model structure is depicted in Fig. 7B. The latter differs from Fig. 7A in that the near-atop CO's have been shifted by ca 0.5Å so to more nearly equalize the CO-CO distances in the unit cell. This model resembles the "distorted hexagonal" (2 x 2) structure deduced for the Rh(111) (2 x 2)-3CO uhv system.¹⁴ At this point, we have no compelling reason to favor the structures in either Fig. 7A or B; a pair of near-atop CO's, consistent with the IRRAS results, are present in both cases. While the latter structure is intuitively more appealing, the greater asymmetry of Fig. 7A might be induced by the presence of the double-layer solvent and/or the cationic countercharge.

It is also worth noting here that the placement of CO molecules in asymmetric atop sites within such high-coverage "compression" structures is consistent with recent Monte Carlo simulations carried out for (111) surface planes.⁷ At least on Pt(111), the frustrated translation of CO within the atop site occurs at a markedly lower frequency than for the twofold bridging geometry, so that displacement away from the former geometry is energetically less demanding.²⁶ Consequently, then, adlayers that favor terminal CO coordination can attain high coverages by forming structures featuring predominantly asymmetric atop sites, thereby minimizing adsorbate-adsorbate repulsive interactions at relatively little cost to the surface-adsorbate binding energies.⁷

We now consider the (3 x √3 rect)-4CO structure, formed at the Rh(111) electrochemical interface at lower electrode potentials. The corresponding infrared spectra (Fig. 2) exhibit a band at 2010-2025 cm⁻¹, indicative of atop (or near-atop) CO, as before, along with a more dominant band at frequencies, 1885-1900 cm⁻¹, intermediate between those characteristic of atop and symmetric twofold coordination geometries. The latter is therefore suggestive of the

predominant presence of CO in an "asymmetric twofold bridging" geometry. The integrated intensity of the former band is about threefold smaller at potentials where the $(3 \times \sqrt{3})$ structure dominates than the corresponding bands at potentials where the (2×2) adlayer is present (Fig. 2). Given that the atop CO coverage, $\theta_{\text{CO}}^{\text{t}}$, in the (2×2) structure equals 0.5, the corresponding $\theta_{\text{CO}}^{\text{t}}$ value in the $(3 \times \sqrt{3})$ adlattice is deduced to be ca 0.15 to 0.2. Since the overall CO coverage in the latter is 0.67, this suggests that only one of the four CO's in the $(3 \times \sqrt{3})$ unit cell is in an atop-type site.

Extracting the precise coordination geometry of the remaining three CO molecules is less clearcut. Although the high intensity of the 1885–1900 cm^{-1} feature is suggestive of a preponderance of CO in an "asymmetric bridging" geometry, relating site occupancies from relative band absorbances is unreliable in the absence of infrared absorptivity (or dynamic dipole moment) information. Moreover, the frequency of the 1885–1900 cm^{-1} band is not necessarily a reliable indicator of the precise site geometry. This is because the ν_{CO} frequency for bridging CO, $\nu_{\text{CO}}^{\text{b}}$, is known to be sensitive to the site occupancy, substantial (up to ca 100 cm^{-1}) upshifts in $\nu_{\text{CO}}^{\text{b}}$ being observed with increasing θ_{CO} for structures where bridging coordination predominates.^{10b} (These frequency upshifts are associated in part with dipole-dipole coupling.^{10b,27}) Consequently, at least a portion of the ca 100 cm^{-1} higher frequency of the "asymmetric bridging" band compared with that anticipated for the symmetric twofold bridging feature at the same potentials can be due to the effects of increased bridging site occupancy in the $(3 \times \sqrt{3})$ compared with the (2×2) structure, rather than to a substantial difference in CO binding geometry.

Turning now to the corresponding STM data, the brightest spot in the $(3 \times \sqrt{3})$ image in Fig. 5A, appearing at the corners of the unit cell as drawn, can be ascribed on the basis of the preceding arguments to the single atop CO.

A suggested topview "ball-model" structure following from this assignment is depicted in Fig. 8. Placing the other three CO's in the unit cell at roughly equal distances from each other, compatible with the spots in the STM images (Fig. 5), yields a pair of CO's in an asymmetric bridging geometry, present inside the unit cell shown in Fig. 8. The positioning of these two CO's is consistent with the appearance of the "asymmetric bridging" feature in the infrared spectra. Although moving the adsorbate from the symmetrical twofold site incurs significant energy cost, this is presumably offset by the resulting diminution in adsorbate-adsorbate repulsion energy.

The positioning of the fourth, and final, CO is more debatable. In Fig. 8, it is placed in a symmetrical twofold site, to be most consistent with stereochemical considerations. The absence of a detectable infrared feature at the frequencies, ca 1770-1800 cm^{-1} , expected for such a symmetrical twofold CO might be considered as evidence against this assignment. However, the absence of this band may be due to the effects of dipole coupling. Provided that the band frequency of the symmetrical bridging CO is suitably close to (say within ca 50 cm^{-1} of), yet lower than, ν_{CO}^b for the "asymmetric" coordination, intensity transfer into the higher-frequency partner can occur, hence attenuating the symmetrical bridging band (cf refs. 7,28). However, given the typically "asymmetric" form of the (3 x 3) STM images, it is tempting to shift this latter CO also to a slightly off-center bridging position. Such a structure might be engendered by coadsorption of water, hydrogen, or possibly by the presence of supporting electrolyte cations. Arguments along these lines, however, are too speculative to be considered further at present.

The (3 x 3 rect) structure has not been observed for Rh(111) in uhv. This is unsurprising since atop rather than bridging CO coordination is generally favored on Rh(111) in uhv in the absence of coadsorbates.^{6a} A markedly increased

propensity for bridging CO binding on Rh(111) is obtained for surfaces preposed with potassium,²⁹ consistent with the marked decreases in work function occurring under these conditions.^{4a} A (3 x $\sqrt{3}$ rect) structure for CO on Pt(111) has been predicted by Monte Carlo calculations;⁷ however, this structure refers to predominantly atop CO coordination.

CONCLUDING REMARKS

While some ambiguities remain, the foregoing is considered to provide a benchmark demonstration of the virtues of STM and IRRAS as complementary in-situ molecular-level probes of ordered adlayer structure at metal-solution interfaces. It should apparently be feasible to obtain STM images of CO and other adlattices in uhv. Such real-space data would be of considerable interest, providing not only a direct comparison with electrochemical STM results but also with structures derived from LEED. The singular example of such STM data in uhv reported so far is CO coadsorbed with benzene on Rh(111).³⁰ Although only the latter coadsorbate was detected in the original published images,^{30a} weak protrusions attributed to CO present in threefold hollow sites were observed subsequently.^{30b} Interestingly, the latter STM images are nicely consistent with the adlattice structure as deduced by dynamical LEED.^{30b} The availability of high-quality vibrational spectra for CO adlayers in both electrochemical and uhv environments provides a major incentive to pursue such STM measurements further at both types of interface.

Some likely limitations of, and unresolved issues in, such studies should be noted. In particular, the STM probe will probably be restricted to the examination of CO (or coadsorbate) adlayers at near-saturation coverages, at least at ambient temperatures, so that sufficiently immobile lattices are formed to allow atomic-resolution images to be obtained. An additional limitation is that it is not clear that the form of the STM images can necessarily be connected

precisely to the spatial position of surface-bound atoms, especially in the case of molecular adsorbates. Even in the case of a simple diatomic molecule such as CO, then, the nature of the STM image may be affected by the adsorbate orientation and electronic bonding properties in a fashion that is yet to be understood. As exemplified here, however, the information on binding site occupancies supplied by IRRAS constitutes the critical element not only in corroborating the STM data, but enabling the real-space structures to be matched to definite CO coordination geometries. In this regard, then, the vibrational spectra fulfills the same role in conjunction with STM as is the case with LEED structural data.

It is interesting to note that a related (2 x 2) structure to that for the present Rh(111) system, with $\theta_{\text{CO}} = 0.75$, has also been observed by using STM for CO on Pt(111) in 0.1 M HClO₄.³ However, the images on Pt(111) differ somewhat from those for the present (2 x 2) structure on Rh(111), the former by themselves being suggestive of adsorption on a single type of site.^{3a} Further detailed studies combining STM and IRRAS on this and other surfaces should yield substantial insight into the factors controlling, as well as the nature of, such adlayer structures.

ACKNOWLEDGMENTS

We are grateful to Dr. M. Van Hove for helpful advice regarding his LEED structures. SCC acknowledges a fellowship from the W.R. Grace Foundation. This work is supported by a grant from the National Science Foundation and the Office of Naval Research (to MJW).

REFERENCES

1. For recent reviews, see for example: (a) Hubbard, A.T., Chem. Rev., 1988, 88, 633; (b) Kolb, D.M., Z. Phys. Chem. N.F., 1987, 154, 179.
2. Yau, S.-L.; Vitus, C.M.; Schardt, B.C., J. Am. Chem. Soc., 1990, 112, 3677.
3. (a) Yau, S.-L., Ph.D. Thesis, Purdue University, 1990; (b) Yau, S.-L.; Schardt, B.C., in preparation.
4. For recent overviews, see: (a) Chang, S.-C.; Weaver, M.J., J. Phys. Chem., submitted (Feature Article); (b) Chang, S.-C.; Roth, J.D.; Ho, Y.; Weaver, M.J., J. Electron. Spect. Related Phenom., 1990, 54/5, 1185.
5. For a review, see: Parsons, R.; Vandernoot, T., J. Electroanal. Chem., 1988, 257, 9.
6. (a) Biberian, J.P.; Van Hove, M.A., Surface Science, 1984, 138, 361; (b) Biberian, J.P.; Van Hove, M.A., Surface Science, 1982, 118, 443.
7. Persson, B.N.J.; Tüshaus, M.; Bradshaw, A.M., J. Chem. Phys., 1990, 92, 5034.
8. (a) Leung, L.-W.H.; Wieckowski, A.; Weaver, M.J., J. Phys. Chem., 1988, 92, 6985; (b) Chang, S.-C.; Leung, L.-W.H.; Weaver, M.J., J. Phys. Chem., 1989, 93, 5341.
9. (a) Chang, S.-C.; Weaver, M.J., J. Chem. Phys., 1990, 92, 4582; (b) Chang, S.-C.; Weaver, M.J., J. Phys. Chem., 1990, 94, 5095; (c) Chang, S.-C.; Weaver, M.J., Surface Science, 1990, 230, 222.
10. (a) Leung, L.-W.H.; Chang, S.-C.; Weaver, M.J., J. Chem. Phys., 1989, 90, 7426; (b) Chang, S.-C.; Weaver, M.J., J. Electroanal. Chem., 1990, 285, 263.
11. Chang, S.-C.; Weaver, M.J., Surface Science, 1990, 238, 142.
12. (a) Chang, S.-C.; Weaver, M.J., Surface Science, in press; (b) Chang, S.-C.; Roth, J.D.; Weaver, M.J., Surface Science, in press.
13. Melandru, S.P.; Anderson, A.B., J. Phys. Chem., 1989, 93, 2044.
14. (a) Van Hove, M.A.; Koestner, R.J.; Somorjai, G.A., Phys. Rev. Lett., 1983, 50, 903; (b) Van Hove, M.A.; Koestner, R.J.; Frost, J.C.; Somorjai, G.A., Surface Science, 1983, 129, 482.

15. Hourani, M.; Wasberg, M.; Rhee, C.; Wieckowski, A., *Croat. Chem. Acta.*, in press.
16. Hourani, M.; Wieckowski, A., *J. Electroanal. Chem.*, 1987, 227, 259.
17. Schardt, B.C.; Yau, S.-L.; Rinaldi, F., *Science*, 1989, 243, 1050.
18. Schardt, B.C., *Rev. Sci. Inst.*, in press.
19. Chang, S.-C.; Yau, S.-L.; Schardt, B.C.; Weaver, M.J., *J. Phys. Chem.*, in press.
20. (a) Corrigan, D.S.; Weaver, M.J., *J. Phys. Chem.*, 1986, 90, 5300; (b) Corrigan, D.S.; Weaver, M.J., *Anal. Chem.*, 1987, 59, 2252.
21. For example, see: (a) Lambert, D.K., *J. Chem. Phys.*, 1988, 89, 3847; (b) Anderson, A.B., *J. Electroanal. Chem.*, 1990, 280, 37.
22. (a) Dubois, L.H.; Somorjai, G.A., *Surface Science*, 1980, 91, 514; (b) Crowell, J.E.; Somorjai, G.A., *Appl. Surface Science*, 1984, 19, 73; (c) Root, T.W.; Fisher, G.B.; Schmidt, L.D., *J. Chem. Phys.*, 1986, 85, 4687.
23. The ν_{CO} -surface potential plot for bridging CO shown in Fig. 2A of ref. 4b contains a frequency value of 1855 cm^{-1} for the Rh(111)/CO($\theta_{\text{CO}} = 0.75$) uhv system, taken from ref. 23b. Frequencies closer to the extrapolated electrochemical value of 1870 cm^{-1} , however, are reported in ref. 22a (1870 cm^{-1}) and 22c (1860 cm^{-1}).
24. For a recent overview, see: Avouris, P., *J. Phys. Chem.*, 1990, 94, 224b.
25. Doyen, G.; Drakova, D. Kopatzki, E.; Behm, R.J., *J. Vac. Sci. Technol.*, 1988, A6, 327.
26. Schweizer, E.; Persson, B.N.J.; Tüshaus, M.; Hoge, D.; Bradshaw, A.M., *Surface Science*, 1989, 215, 49.
27. For example, see: (a) Hoffman, F.M., *Surface Science Reports*, 1983, 3, 107, (b) Ortega, A., Hoffman, F.M.; Bradshaw, A.M., *Surface Science*, 1982, 119, 79.
28. For explanative discussions of such "intensity-transfer" effects, see: (a) Hollins, P.; Pritchard, J., *Prog. Surface Science*, 1985, 19, 275; (b) Tüshaus, M.; Schweizer, E.; Hollins, P.; Bradshaw, A.M., *J. Electron. Spect. Related Phenom.*, 1987, 44, 305.
29. Crowell, J.E.; Somorjai, G.A., *App. Surface Science*, 1984, 19, 73.

30. (a) Ohtani, H.; Wilson, R.J.; Chiang, S.; Mate, C.M., *Phys. Rev. Lett.*, 1988, 60, 2398; (b) Chiang, S.; Wilson, R.J.; Mate, C.M.; Ohtani, H., *J. Microscopy*, 1988, 152(2), 567.

FIGURE CAPTIONSFig. 1

Cyclic voltammograms for ordered Rh(111) crystal in 0.1 M HClO₄, at 50 mV s⁻¹. Solid trace: electrooxidation of irreversibly adsorbed CO, preadsorbed at -0.25 V vs SCE. Dashed trace: typical voltammogram obtained after CO removal, after 10 cycles between -0.25 V and 0.55 V.

Fig. 2

Sequence of infrared absorbance spectra in the 1750-2150 cm⁻¹ region for adsorbed CO on Rh(111) in CO-saturated 0.1 M NaClO₄, obtained during positive-going potential sweep at 1 mV s⁻¹ from -0.4 V vs SCE. Each spectrum involved acquiring 100 interferometer scans (consuming ca 1 min), subtracted from which was a similar set of scans acquired after complete CO electrooxidation.

Fig. 3

In-situ topview atomic-resolution STM image of Rh(111) substrate. Image acquired in CO-containing 0.1 M NaClO₄ at 0.5 V vs SCE using -17.7 mV tip-surface bias voltage (V_b) and 15 nA set-point current (i_t). A 2d Fourier transform filter utility (Nanoscope II software) was utilized to "remove" noise closer than 2Å.

Fig. 4

- A. An unfiltered 80 x 80Å topview STM image of the Rh(111)-(2 x 2)-3CO structure, obtained with $V_b = 1.8$ mV, $i_t = 45$ nA in CO-saturated 0.1 M NaClO₄ at -0.1 V vs SCE.
- B. A magnified (zoom-in) 25 x 25Å portion of A after Fourier transform filtering.
- C. Three-dimensional "height-shaded surface plot" of image in Fig. 4, with viewpoint 30° off the surface normal.
- D. A 25 x 25Å portion of another, unusually clearly resolved, (2 x 2) domain, obtained with $V_b = -15$ mV, $i_t = 15$ nA in CO-saturated 0.1 M NaClO₄ at -0.1 V vs SCE.
- E. "Height-shaded surface plot" of D, drawn as in C.

Fig. 5

- A. Filtered 25 x 25Å topview STM image of Rh(111)-(3 x √3 rect)-4CO structure, obtained with $V_b = 166$ mV, $i_t = 9$ nA in CO-saturated 0.1 M NaClO₄ at -0.3 V vs SCE.
- B. Three-dimensional "height-shaded surface plot" of image in Fig. 5A.
- C. Filtered topview STM image of two adjacent, yet 60° rotated domains of (3 x √3 rect) structure on same Rh(111) terrace, obtained with $V_b = 200$

mV, $i_t = 20$ nA in CO-saturated 0.1 M NaClO₄ at -0.3 V vs SCE.

D. As for C, but for third rotational domain of (3 x √3 rect) structure, with $V_b = 200$ mV, $i_t = 5$ nA.

Fig. 6

Filtered topview STM image of domain boundary region between the (2 x 2) and (3 x √3 rect) adlayer structures, obtained with $V_b = 50$ mV, $i_t = 10$ nA in CO-saturated 0.1 M NaClO₄ at -0.25 V vs SCE.

Fig. 7

Proposed pair of topview "ball-models" for (2 x 2)-3CO adlayer at Rh(111)-aqueous interface. The top-layer Rh atoms are depicted as the larger circles, with smaller circles representing position of individual CO molecules (see text for details).

Fig. 8

As for Fig. 7, but for (3 x √3 rect)-4CO adlayer at Rh(111)-aqueous interface (see text for details).

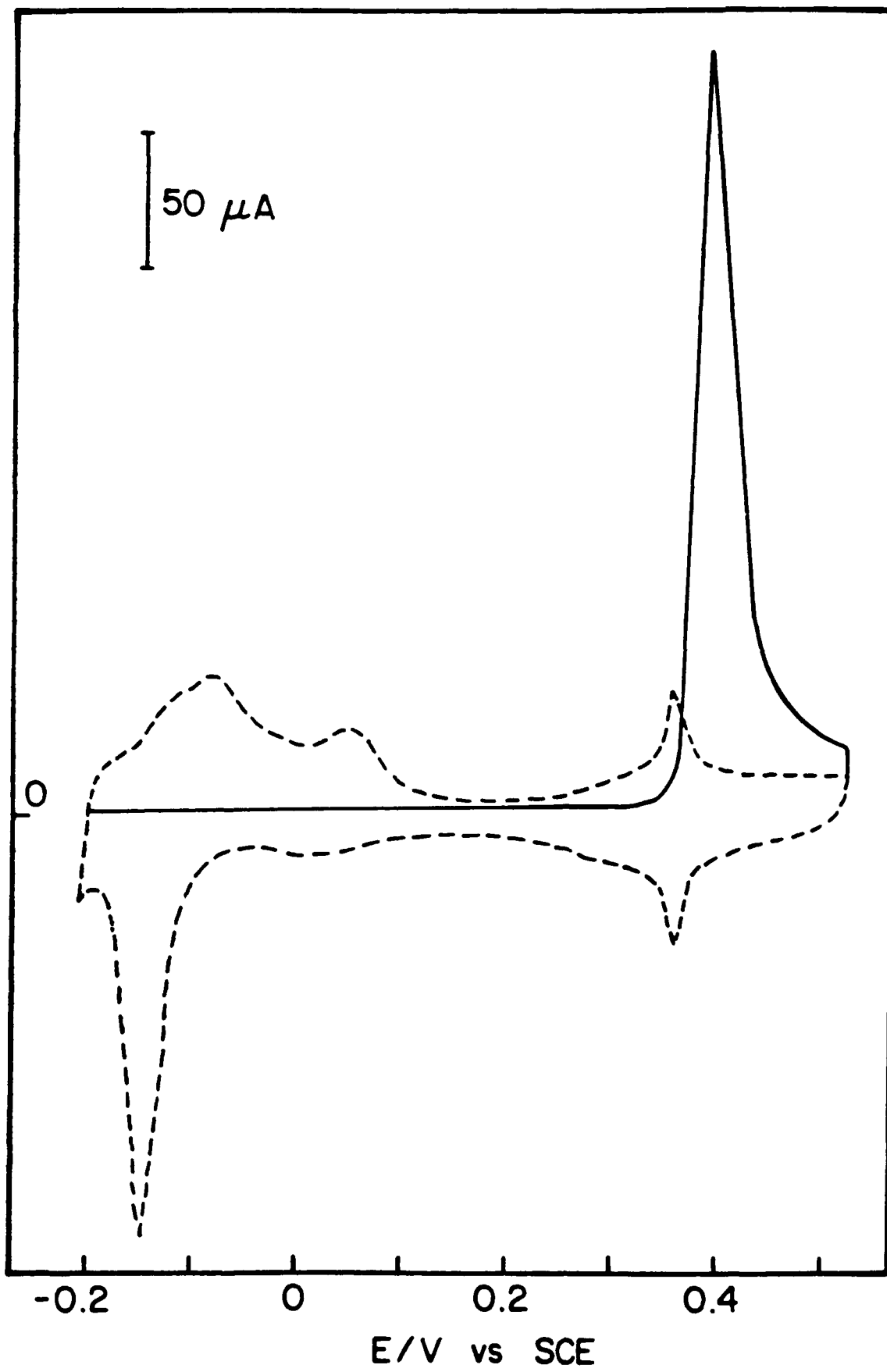


Fig. 1

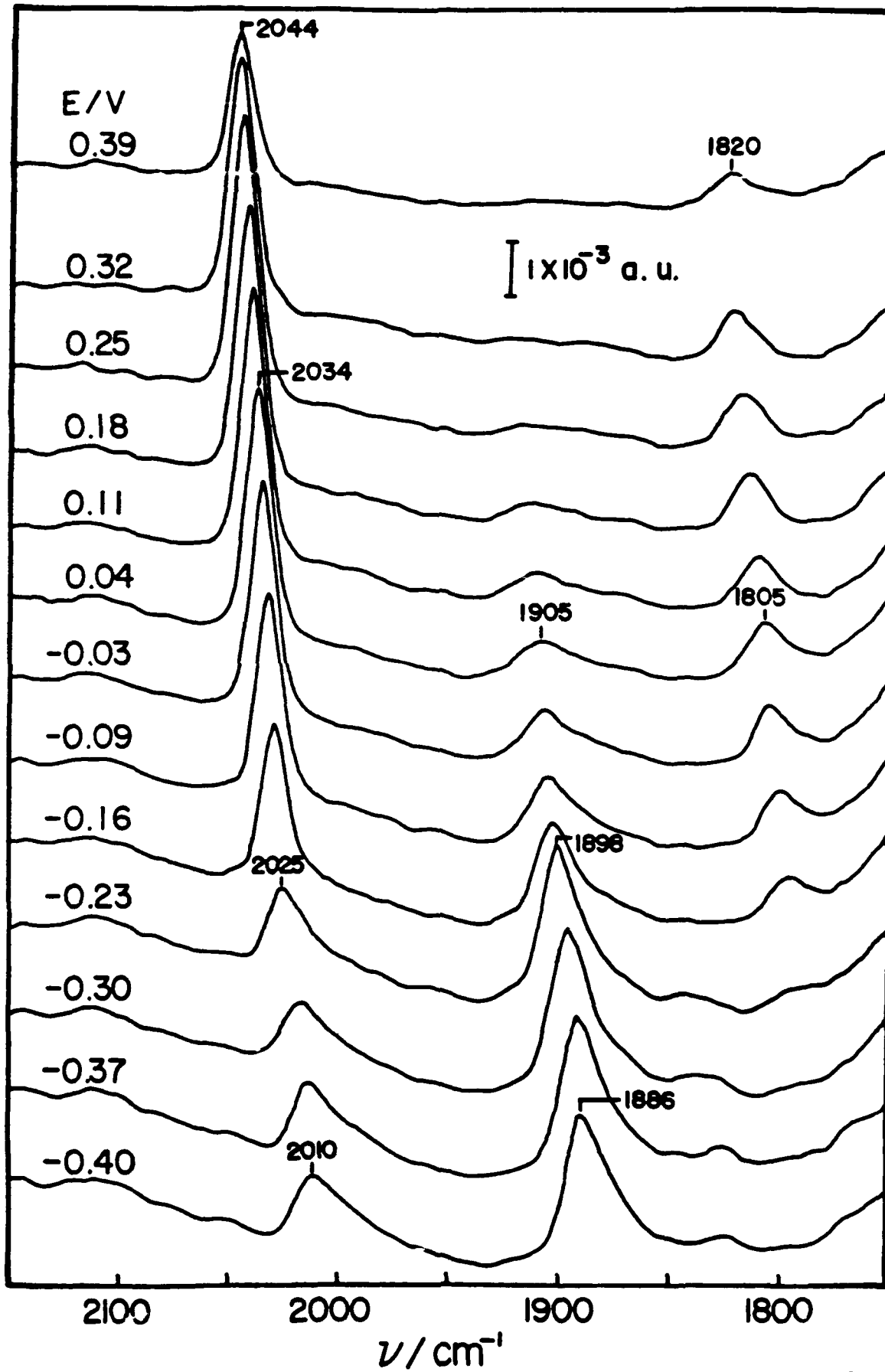


Fig. 2

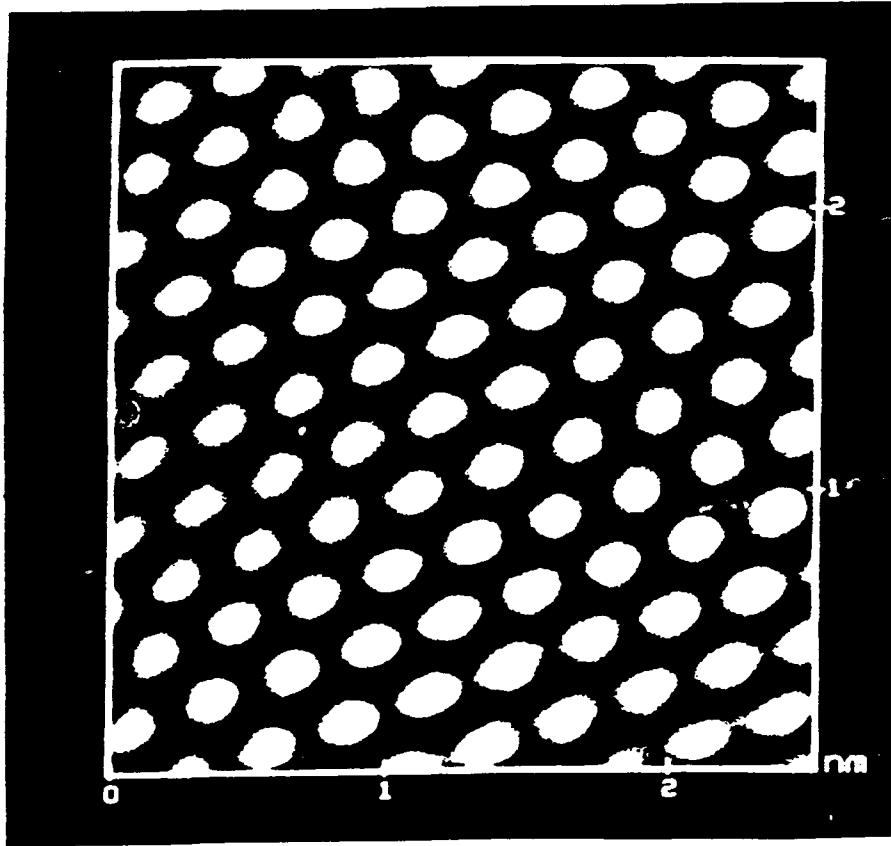


Fig. 3

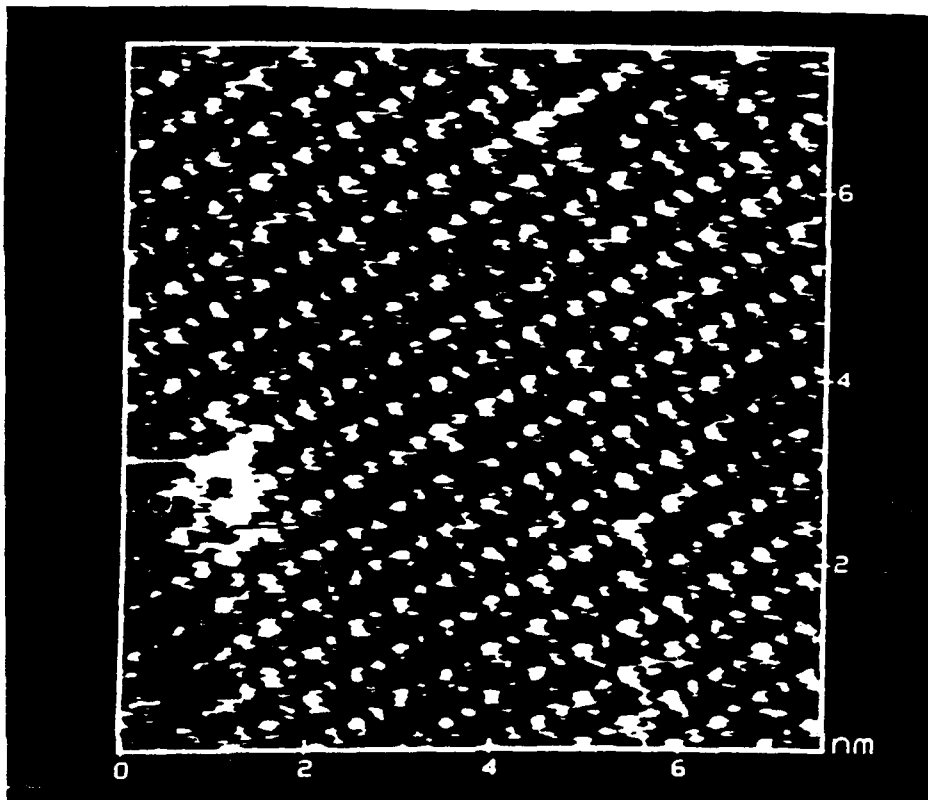


Fig 4A

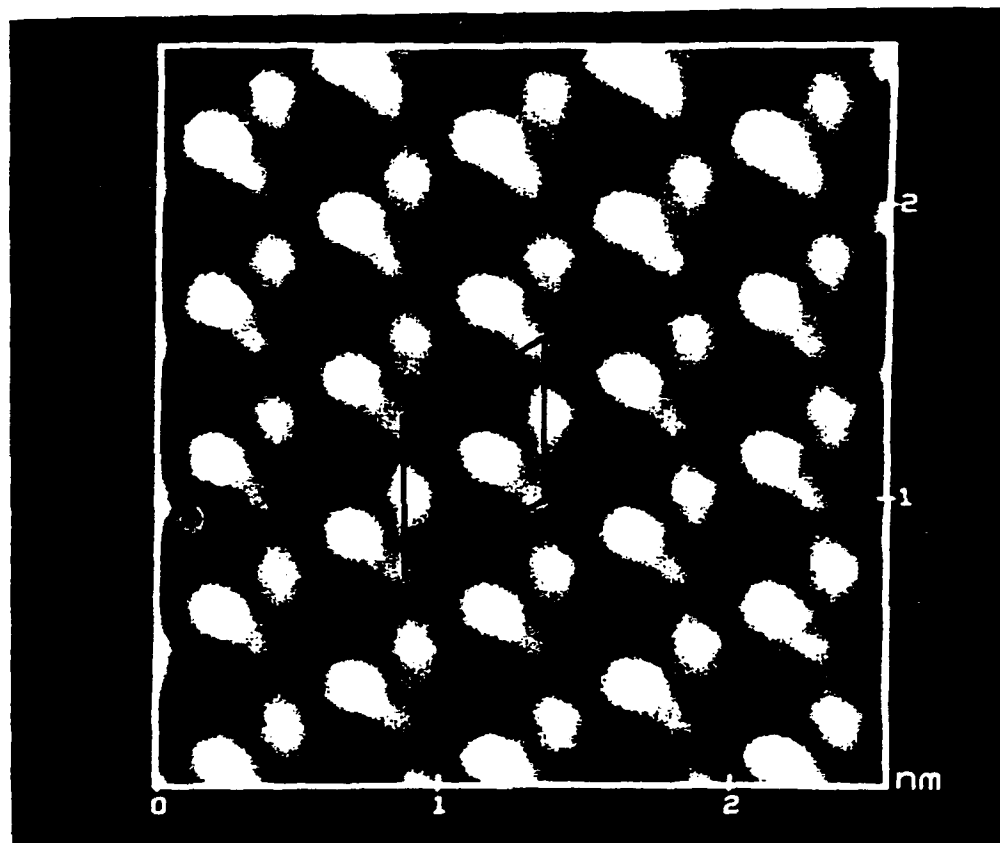


Fig. 4B

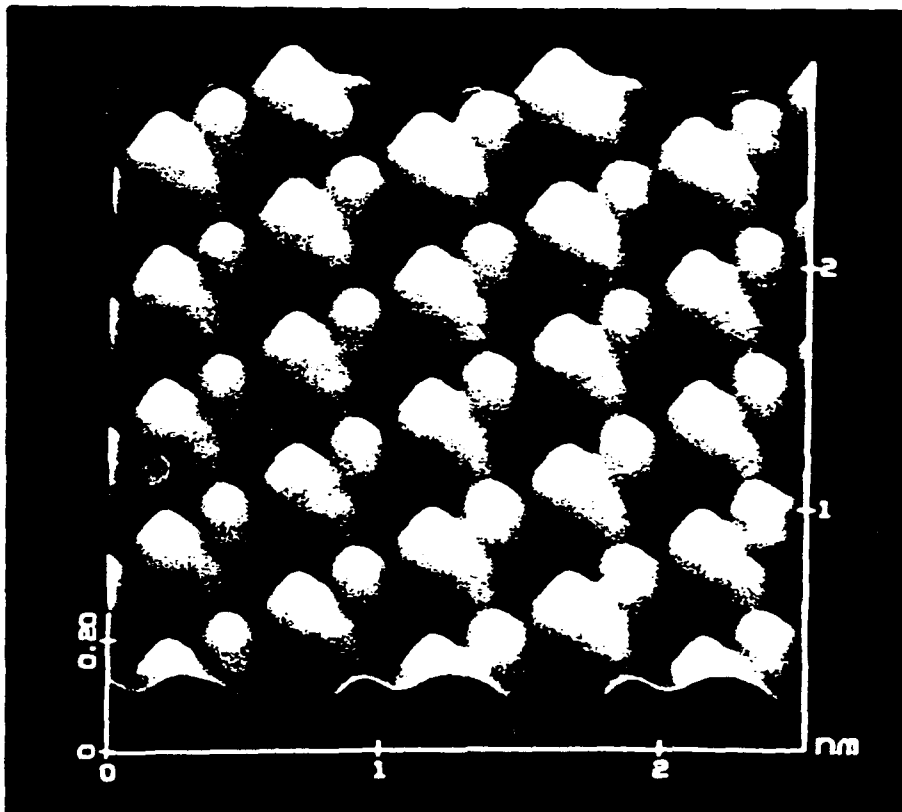


Figure 4C

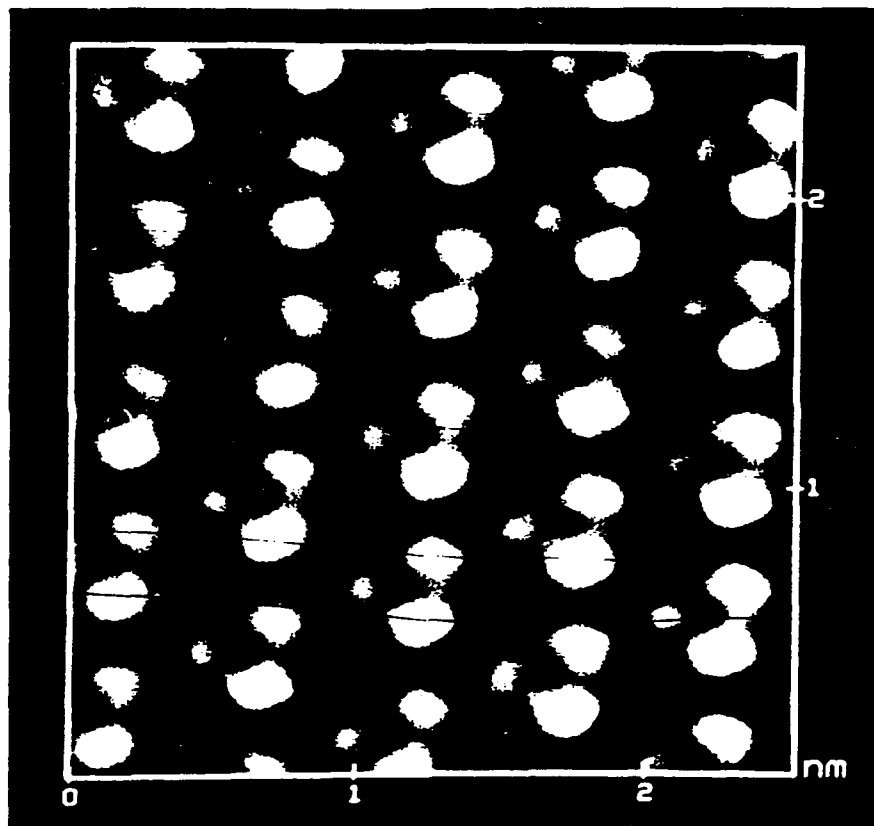


Fig. 4D

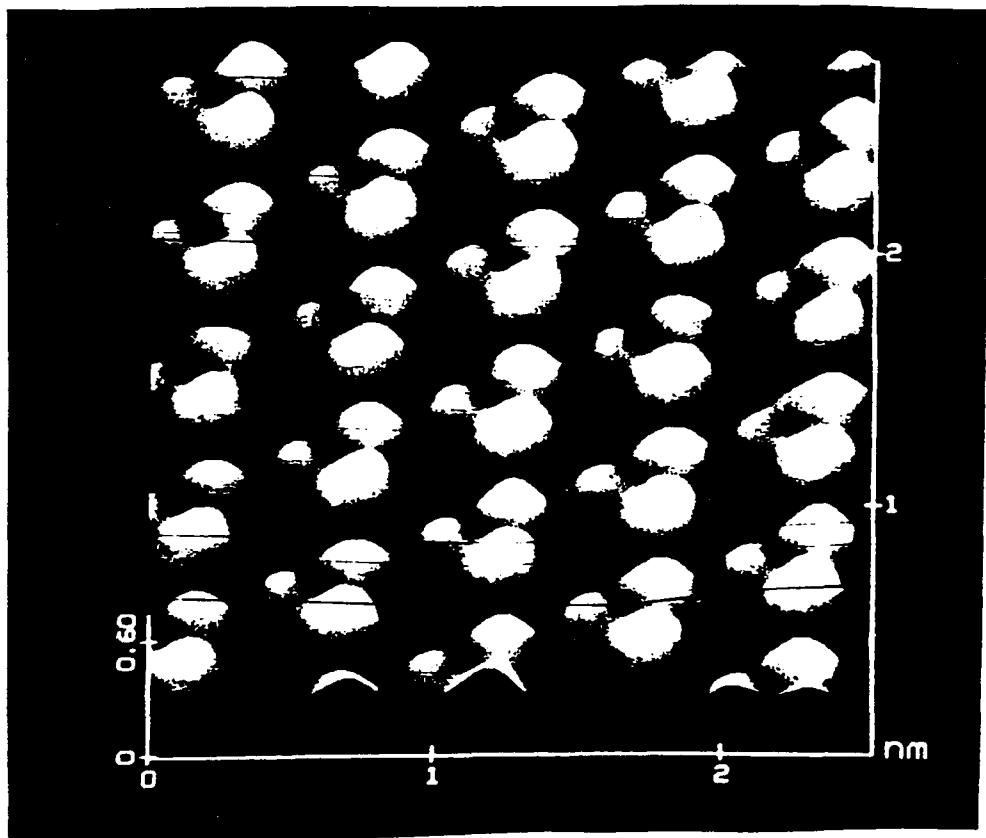


Fig. 4E

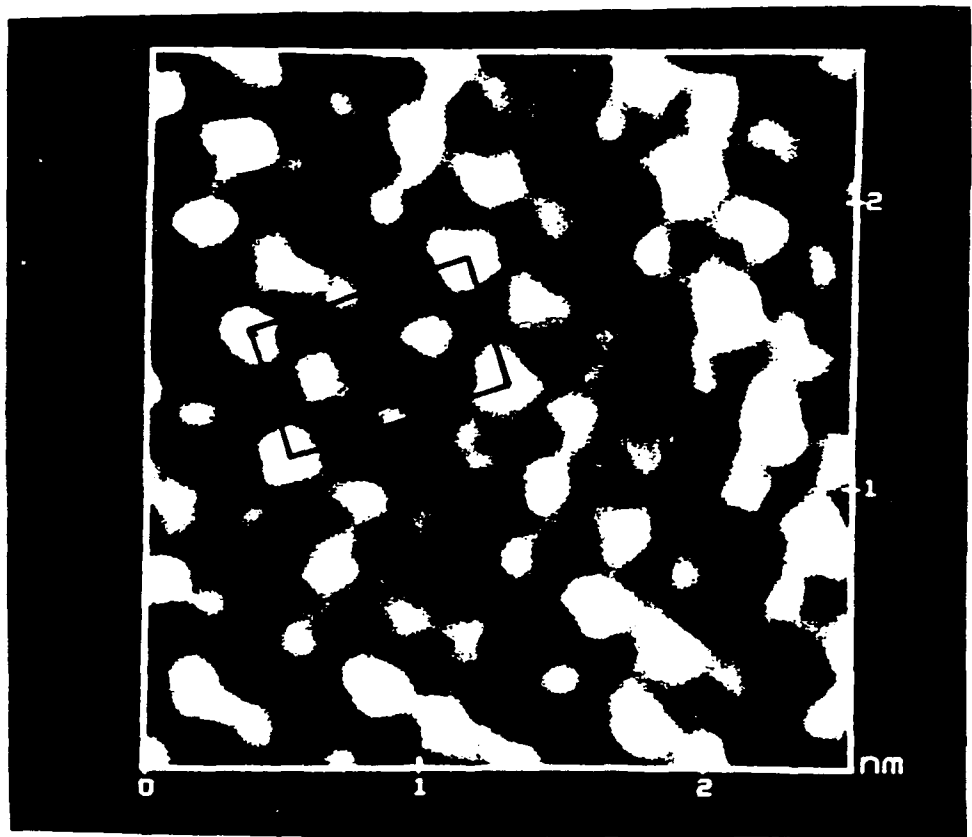


Fig. 5A

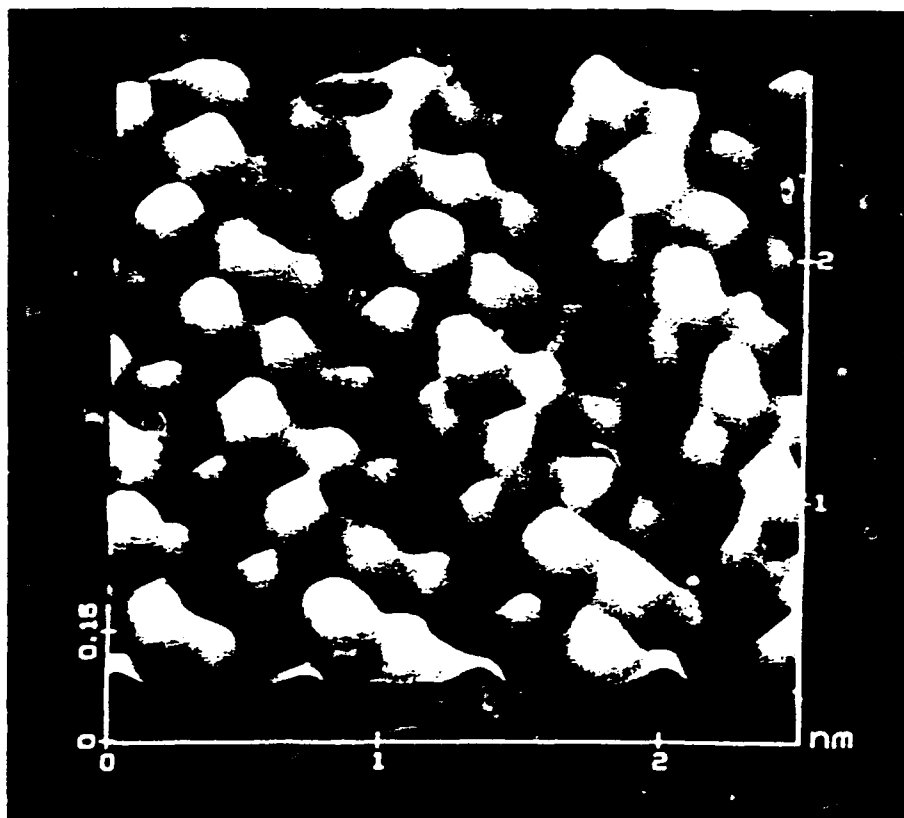


Figure 5B

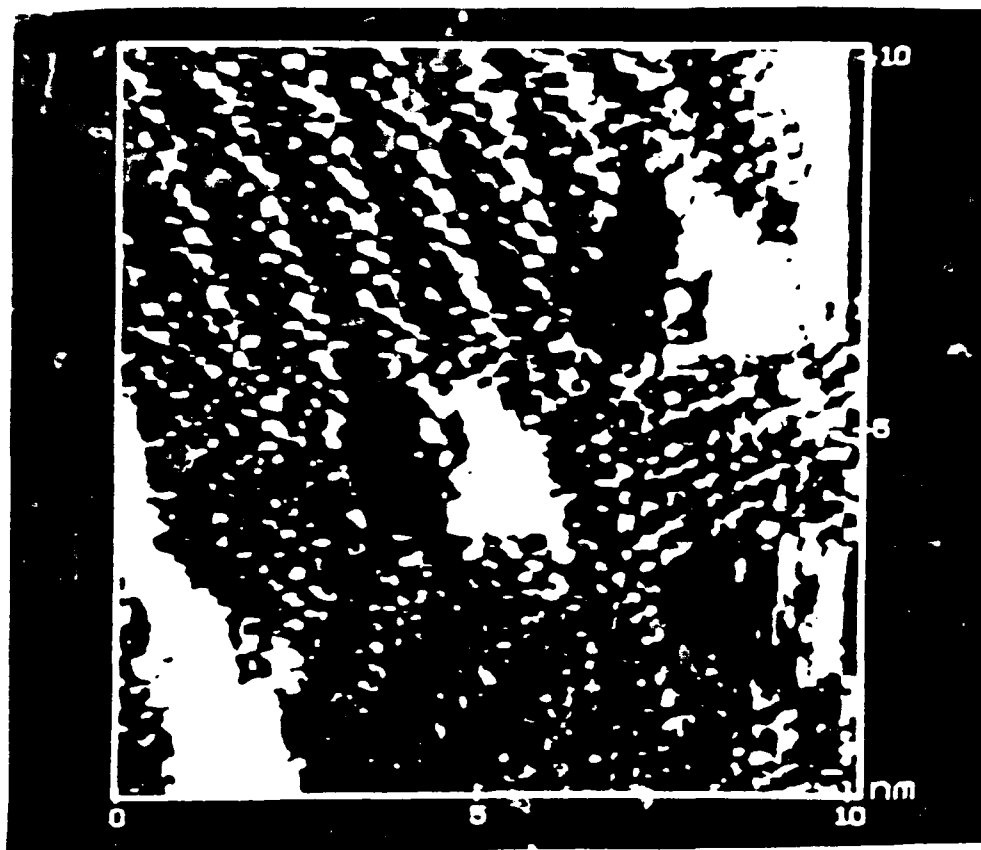


Fig. 5C

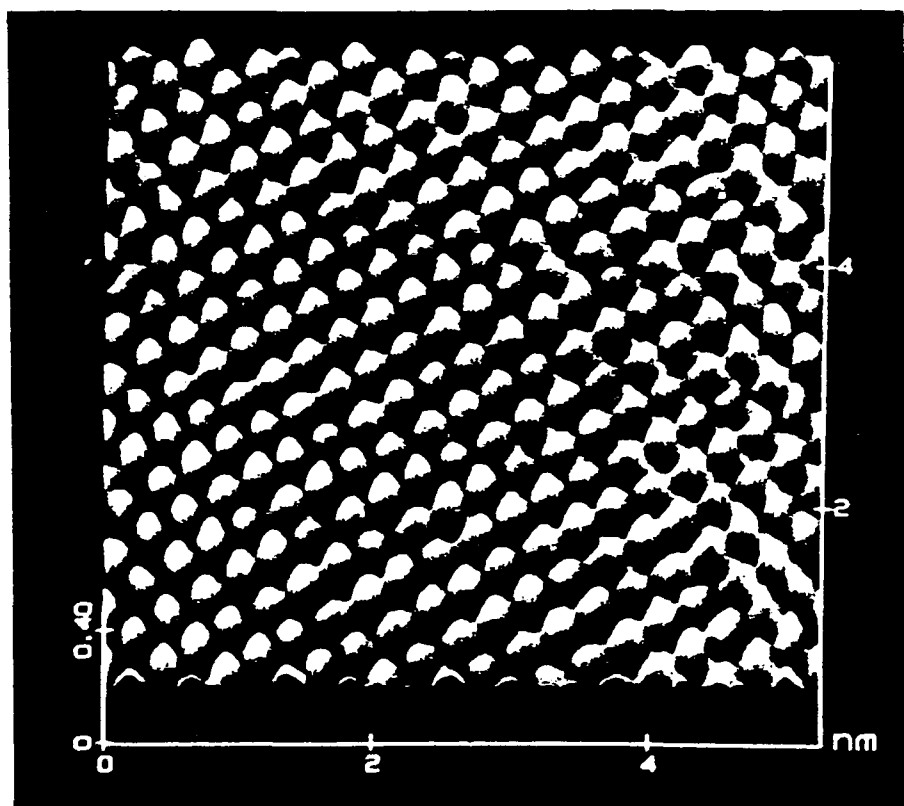


Figure 5D

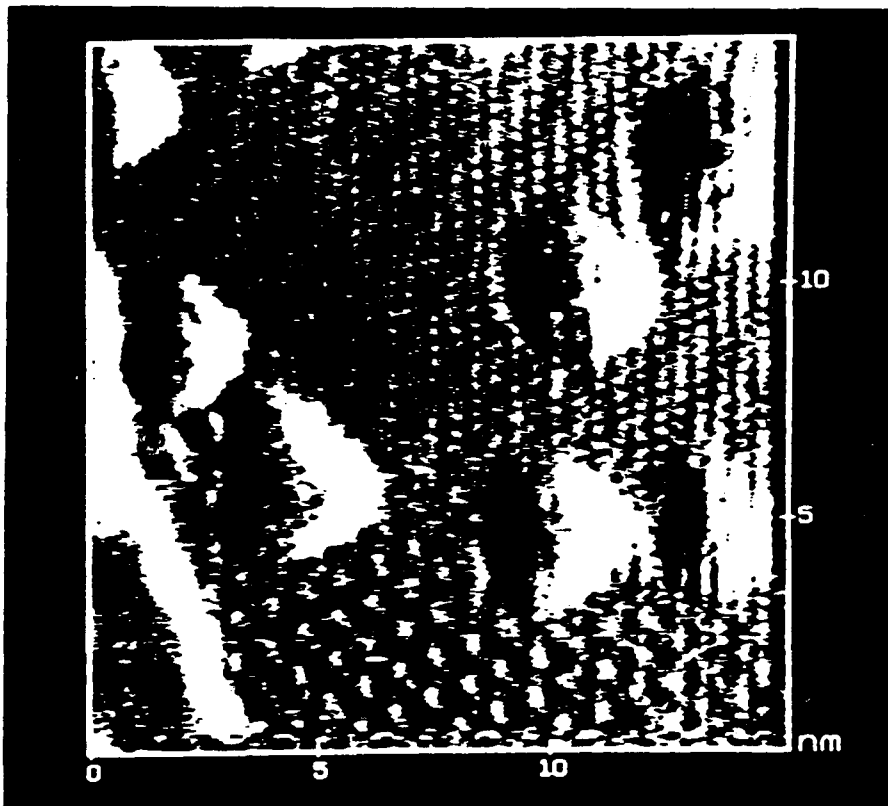


Figure 6

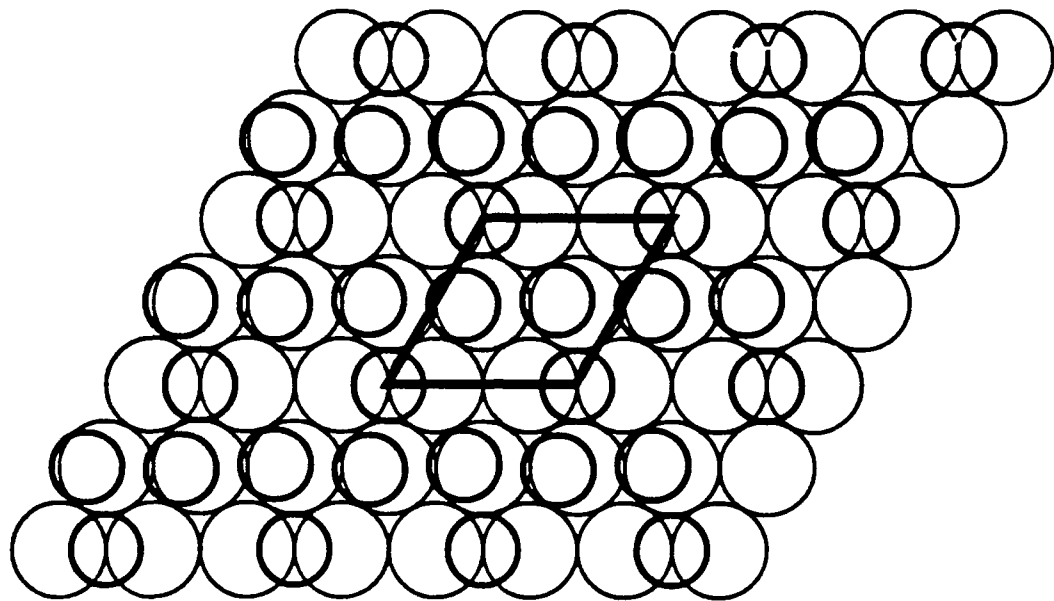


Fig 7A

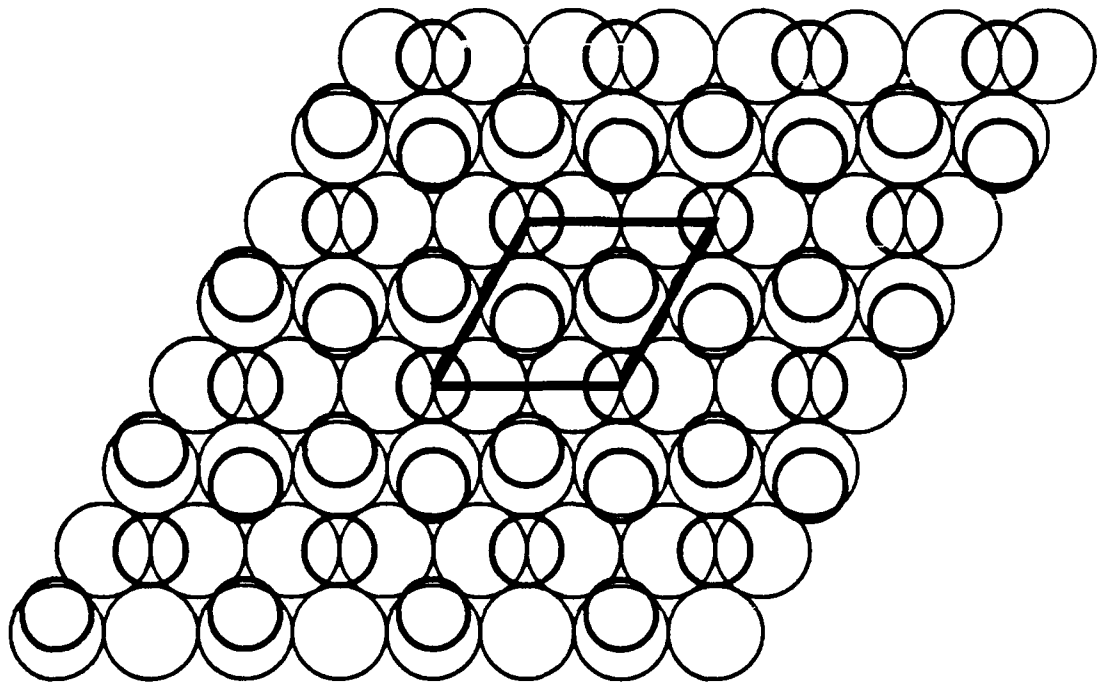


Fig. 7B

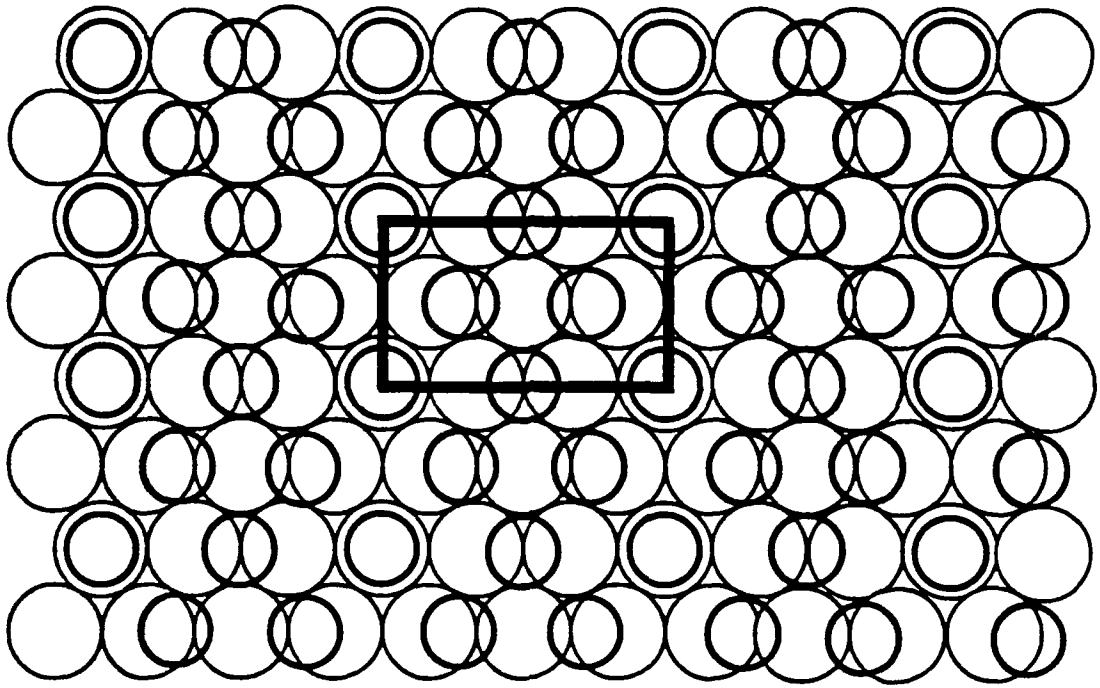


Fig. 8

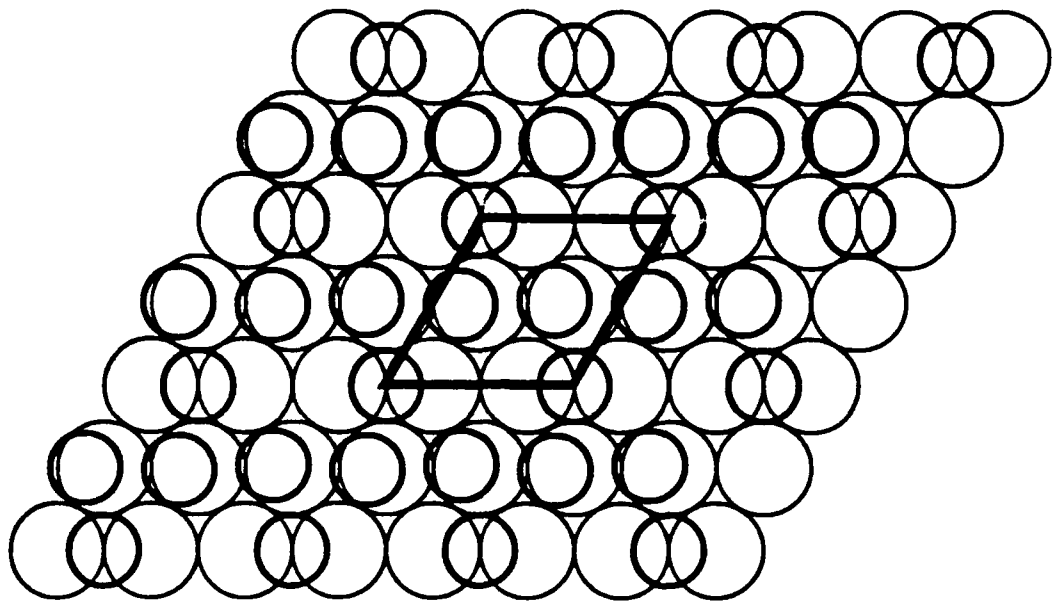


Fig 7A

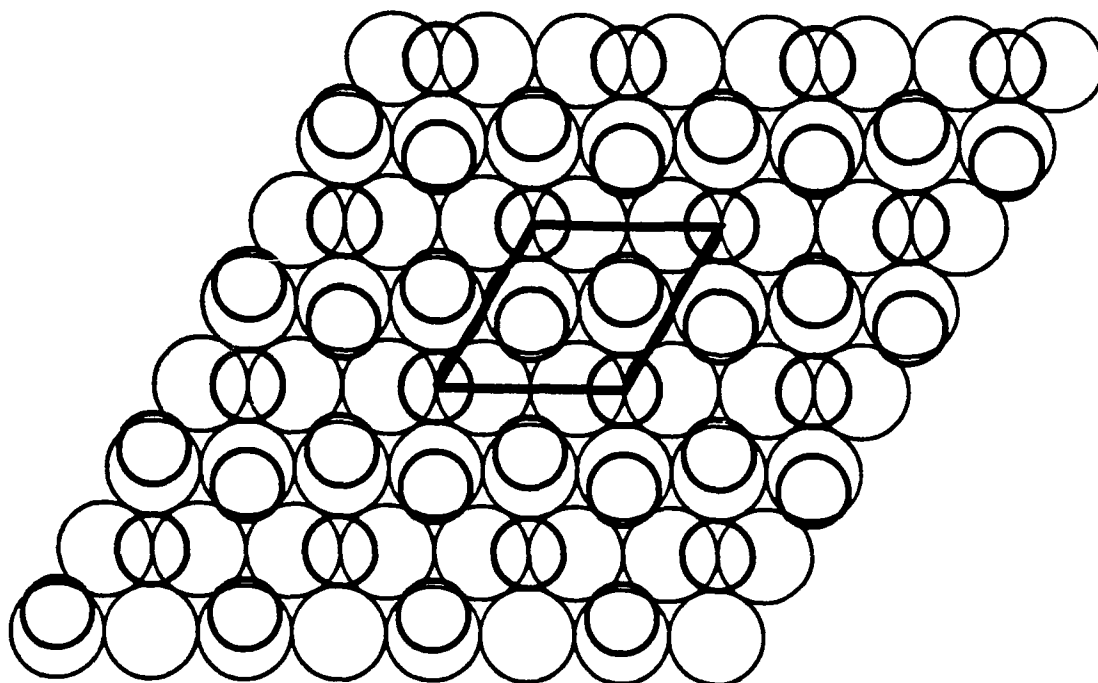


Fig. 7B

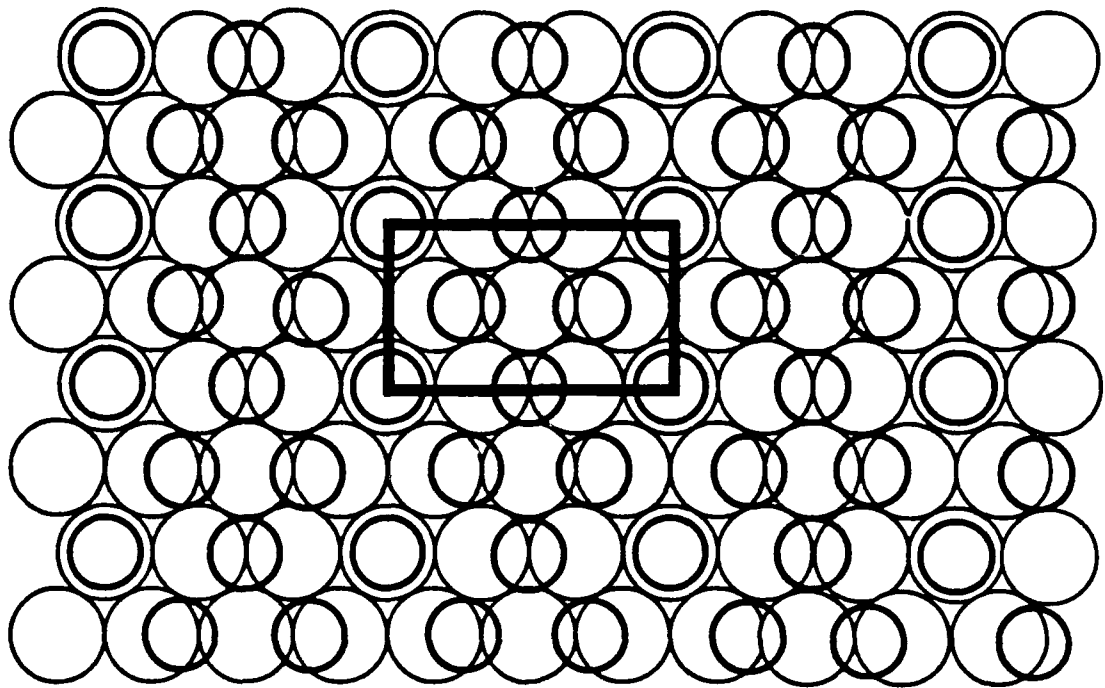


Fig. 8